Damping identification based on a high-speed camera

I. Tomac[a,*], J. Slavič[b,*]

[a] *University of Split, Faculty of Electrical Engineering, Mechanical Engineering and Naval Architecture, Ruđera Boškovića 32, 21000 Split, Croatia*
[b] *University of Ljubljana, Faculty of Mechanical Engineering, Aškerčeva cesta 6, 1000 Ljubljana, Slovenia*

Cite as:
Ivan Tomac, Janko Slavič; Damping identification based on a high-speed camera, Mechanical Systems and Signal Processing, Volume 166, March 2022,
https://doi.org/10.1016/j.ymssp.2021.108485

Abstract

Monitoring distant structures using a high-speed camera frequently relies on modal parameters. Even with high-dynamic-range sensors (*e.g.*, accelerometers) damping identification is not trivial. With high-speed cameras the dynamic range is relatively small and contaminated with a relatively high level of noise. Image-based techniques have the advantage of providing contact-less full-field structural identification. While the damping is a modal parameter and theoretically not spatially dependent, this study looks at the potential to use the spatial over-determination, provided by the high-speed camera to increase the accuracy of the contact-less damping identification. High-speed cameras provide thousands of measurement locations, and identify the damping with noise-resistant methods like those based on the Continuous Wavelet Transform is numerically demanding. This research is built on the the Morlet Wave Damping Identification method, which is based on the Continuous Wavelet Transform, but is also significantly faster. Finally, the full-field damping parameters were averaged with regard to the identified deflection shapes. The theory is extended with an experiment, where damping is identified for a simple structure at frequencies up to 2.5 kHz. It was found that the proposed method resulted in damping identification that was comparably accurate to the damping identified from high-dynamic-range and low-noise piezoelectric accelerometers. This research confirms that damping can be accurately identified from high-speed-camera measurements, only.

Keywords: Morlet-wave, damping, spatial distribution, full-field

*Corresponding author
Email addresses: itomac@fesb.hr (I. Tomac), janko.slavic@fs.uni-lj.si (J. Slavič)

1. Introduction

High-speed cameras are seeing increasing use in the field of structural dynamics [1, 2], where they provide contact-less measurements of displacements with a high spatial resolution. Theoretically, each pixel can be a sensor enabling a full-field measurement [3, 4]. One of the advantages is that high-speed camera measurements offer a full-field response from a distant object [5]. Non-contact and distant monitoring make possible applications that are not possible or hard to perform with conventional approaches, *e.g.*, helicopter blades [6], marine propellers inside cavitation tunnels [7, 8] and wind-turbine blades [9, 10]. Camera-based approaches are also used to monitor concrete structures under seismic loads [11], bridges [12], as well as on-line health monitoring [13]. One of the disadvantages of high-speed camera measurements is the relatively high noise; typically on 8 bit grayscale image sensor has approximately 3 bits of noise [14, 15]. This noise is even more pronounced when reducing the field of view, which is the case with distant objects [16].

In recent years, image-based research has also focused on modal identification. Yang *et al.* [17] proposed output-only procedures based on a blind source separation technique utilising independent component analysis to isolate the vibrating modes and identify mode-shapes from a full-field measurement. Damping is identified using a logarithmic decrement. Yu and Pan [18] researched the use of a single camera for stereo digital image correlation; they also applied a half-power bandwidth method to identify the first three damping ratios on four discrete points of a thin aluminium plate. Huňady *et al.* [19] developed a methodology based on singular-value decomposition to detect mode-shapes and to decouple the physical model by generating weighted frequency-response functions for each mode; the damping is identified using rational fraction polynomial and frequency-domain polynomial methods. Ege *et al.* [20] conducted identification of the loss factor on a multi-layer thin plate using laser Doppler vibrometer up to a high frequency range. Felipe-Sesé *et al.* [21] used the circle-fitting method to identify the modal parameters. To obtain a single natural frequency and damping ratio for each mode, the identified mode-shape amplitudes were used for weighting. Yang *et al.* [22] proposed a data-driven method based on data clustering to blindly identify the natural frequency and perform the mode separation. Silva *et al.* [23] performed a pixel-wise mode decomposition using Nonnegative Matrix Factorization algorithms to generate separate videos for each mode that are then used to identify a mode shapes and natural frequencies using the blind source separation complexity pursuit algorithm; damping is estimated using conventional Fourier-transform and logarithmic decrement techniques. Marchetti *et al.* [24] modeled structural damping of the multi-layer plate and used space domain approach for experimental verification of the structural loss factor in high-frequency range.

The focus of this research is to overcome the relatively noisy measurements obtained with high-speed cameras using the over-determination this full-field measurement provides. At the same time, the damping-identification uncertainty is spatially dependent (higher at the nodes). The damping identification will be based on the Morlet-Wave Damping Identification (MWDI) method [25], which was previously shown to have the advantages of the continuous wavelet transform method (CWT), *e.g.*, identification on short signals,

resistance to noise, good frequency separation, [26, 27]; however, MWDI is numerically significantly less demanding [25, 28].

This manuscript is organized as follows. Sec. 2 gives the theoretical background required in Sec. 3, where the Spatially Weighted Morlet-Wave Damping Identification method is introduced. Experimental research is discussed in Sec. 4. Conclusions are given in Sec. 5.

2. Theoretical background

Here, the theoretical background and prior knowledge required in the subsequent sections will be presented. In particular, the basics on the Morlet-Wave Damping Identification (MWDI) [25] and the Extended MWDI [28] will be described.

2.1. Morlet-Wave damping identification method

The MWDI method is based on the Continuous Wavelet Transform (CWT) damping identification [26, 27, 29]. If the modes are not close, the CWT is able to decompose particular modes and the damping can be identified per particular mode [27]. If the CWT is based on a two-dimensional, time-frequency grid, then the MWDI is based on a finite integral, which is obtained for each mode at one time-frequency point, only. Fig. 1 shows the damped response f_m of a SDOF system that is described with the frequency of oscillation ω (usually easy to identify), the amplitude of oscillation X and damping ratio δ of the viscous damping parameter over critical damping. Similar to the CWT, the MWDI defines the integral I:

$$I(n,k,\omega) = \int_0^T f_\mathrm{m}(t)\,\psi^*(n,k,\omega,t)\,\mathrm{d}t, \tag{1}$$

where T is the time length of the analyzed mode, which is, due to spectral-leakage reasons, defined by the number of oscillations k ($k \in \mathbb{N}$) at the analyzed frequency ω: $T = 2\,\pi\,k/\omega$; * is the complex conjugate and ψ is a Morlet wavelet function [30] expressed with parameters n, k, ω:

$$\psi(n,k,\omega,t) = (2\pi)^{-\frac{3}{4}}\sqrt{\frac{n\omega}{k}}\exp\left[-\left(\frac{n}{4k\pi}\right)^2(k\pi-\omega t)^2 + i\,(k\pi-\omega t)\right] \tag{2}$$

The unknown amplitude X can be reduced, by obtaining the integral I at two different values of the time-spread parameter n:

$$\tilde{M}\,(n_1,n_2,k,\omega) = \frac{|I(n_1,k,\omega)|}{|I(n_2,k,\omega)|}, \tag{3}$$

where effect of n_1 and n_2 parameters on the wavelet-function envelope is shown in Fig. 1. An influence of parameters: n_1, n_2 and k on damping identification is discussed in Subsection 2.1.1.

The ratio $\tilde{M}$ can be obtained from a measurement, but for a SDOF-free response, it can also be defined analytically. If the Eq. (1) is inserted into Eq. (3) and the SDOF-free

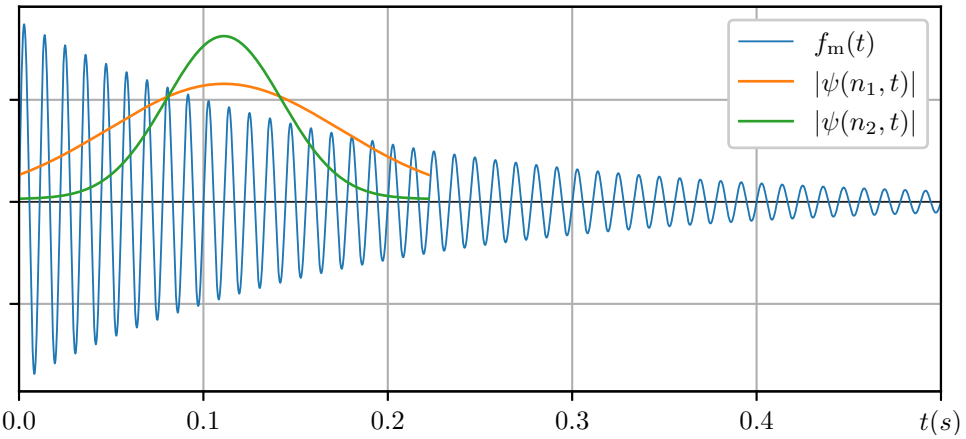

Figure 1: Shape and position of the WFs on a simple example of a decaying signal (for details see Appendix A). WF parameters are: $n_1 : n_2 = 5 : 10$, $k = 20$, $f = 90$ Hz.

response is expressed as $f_{\mathrm{m}}(t) = X \exp(-\delta\omega t) \cos(\omega t - \varphi)$, the ratio is expressed as:

$$M(n_1, n_2, k, \delta) = \frac{\left| \int \cancel{X} \exp(-\delta\omega t) \cos(\omega t - \varphi) \, \psi^*(n_1, k, \omega, t) \, \mathrm{d}t \right|}{\left| \int \cancel{X} \exp(-\delta\omega t) \cos(\omega t - \varphi) \, \psi^*(n_2, k, \omega, t) \, \mathrm{d}t \right|}, \tag{4}$$

it can be seen that constant X is reduced, which is also, the key feature of the MDWI method. The further procedure leads to the analytical expression as [25]:

$$M(n_1, n_2, k_i, \delta_i) = \exp\left(4\pi^2 k_i^2 \delta_i^2 \frac{n_2^2 - n_1^2}{n_1^2 n_2^2}\right) \sqrt{\frac{n_2}{n_1}} \, G(n_1, n_2, k_i, \delta_i) \tag{5}$$

where δ_i is the damping ratio of the i-th mode and G is based on the error functions, see [25]. Damping is identified by solving the equation:

$$\tilde{M}(n_1, n_2, k_i, \omega_i) - M(n_1, n_2, k_i, \delta_i) = 0 \tag{6}$$

for the unknown δ_i.

For $n_1 \geq 10$ and $n_1 < n_2$ Eq. (5) simplifies to $G \approx 1$; in this case the closed-form solution can be obtained. If the simplification on G cannot be made, then the damping is identified by numerically solving Eq. (6). For details, see [25].

2.1.1. MWDI parameter selection and the Extended MWDI method

The time-spread parameter n defines the sensitivity of the MWDI method: the smaller the n_1, the more sensitive is the damping identification, Eq. (5). However, with a smaller n the uncertainty of the identification increases [25]. From previous research, the parameter n_1 is typically selected as 5 (high sensitivity), 7 (medium sensitivity) or 10 (low sensitivity) and the ratio of $n_1 : n_2 = 1 : 2$ is used [25].

The minimal value of k is defined by the admissibility condition for the wavelet function [25, 31]. On the other hand, the maximum k is not clear: a large number of oscillations

would, in general, increase the accuracy; however, as the free response is damped and the level of noise can be considered constant, the signal-to-noise ratio (SNR) decreases with higher k. Further, with high k the frequency spread of the identification also becomes very narrow which increases the uncertainty of the identification if the frequency of the oscillation varies slightly.

The third parameter ω is a frequency of the wavelet function which is set on the natural frequency of the systems. This parameter can be numerically tuned to search for the maximum absolute value of the wavelet coefficient I, Eq. (1). This way an exact natural frequency is identified.

An example of the MWDI method is shown in Fig. 2 ($\delta = 1\,\%$, for other parameters, see Appendix A). It is clear that the selection of the parameters (n_1, n_2 and k) significantly influences the convergence of the identification; high values of n also result in a systematic error [25]. The extended MWDI method presents an optimisation approach to the parameters' selection to achieve a convergent result. The method is originally established for identification of damping from a single measurement point in the whole range of feasible parameters k and n_2. The parameter n_1 is set constant, $n_2 = \{n_2 \in \mathbb{N} : n_1 < n_2 \leq 2n_1\}$ and k is set in range too. The optimisation procedure is consisted of searching for k value that has minimal variation of identified damping for different n_2 values. For details, see Tomac *et al.* [28]. In this research eMWDI is established between different spatial points for a single n_1, n_2 set, details are in the following section.

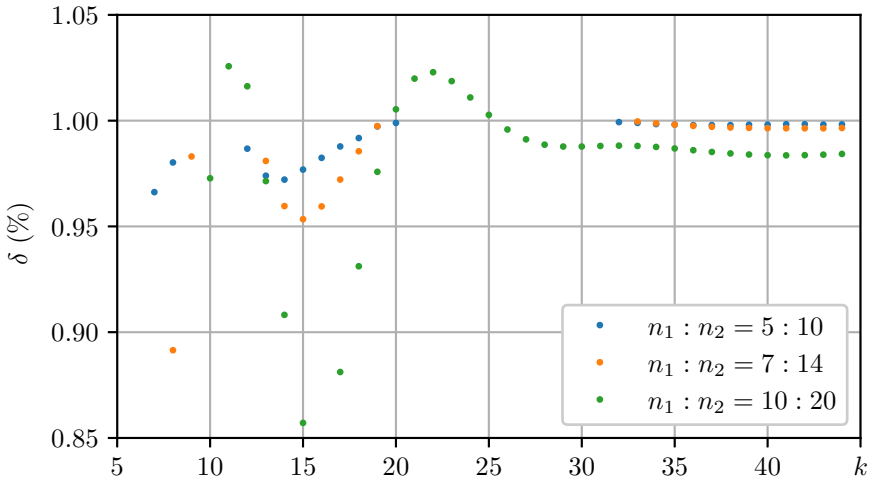

Figure 2: Identified damping vs the parameter k.

3. Spatially weighted Morlet-Wave Damping Identification

MWDI is resistant to noise; however, the noise in camera data is orders of magnitude higher than that in classical piezoelectric accelerometers: a typical 8 bit (grayscale) high-speed camera has 3 bits of noise [15]; in case the of a better, 12 bit, camera the noise is typically 5 bits [32, 33]. Due to the high level of noise, the damping identification with high-speed cameras is especially difficult [4, 21].

This research introduces the MWDI-based method where the spatial over-determination of the damping is used to reduce the uncertainty of the identification. Further, for a particular mode, the SNR is smaller close to the nodes and therefore a spatial weighting is introduced. The proposed spatially weighted MWDI method follows these steps:

1) Identify displacements from image data (optical flow or DiC)
2) Obtain the spatial power spectral density (PSD)
3) Roughly estimate natural frequencies from PSD
4) Identify the exact natural frequencies and search for optimal k parameter using extended MWDI at regions with the highest spectral energy
5) Apply MWDI at all spatial locations
6) Apply spatial weighting

In step 1, the identification of the displacement $f_{\mathrm{m},j}(t)$ at the location j in the time domain is followed by step 2 where the power spectral density (PSD) $P_j(\omega)$ [34] is obtained:

$$P_j(\omega) = \frac{1}{T}\,\hat{f}^*_{\mathrm{m},j}(\omega)\,\hat{f}_{\mathrm{m},j}(\omega), \tag{7}$$

where $\hat{f}_{\mathrm{m},j}(\omega)$ is the Fourier transform and * is the complex conjugate. In step 3, from the spatial PSD $P_j(\omega)$ a rough estimation of the natural frequencies ω_i is made; i is the mode index.

In step 4, the rough natural frequencies are used at locations with high PSD values (*e.g.* the top 1%) to perform the extended MWDI, where the search for parameter $k \in \mathbb{N}$ and $k_{\mathrm{lo}} \leq k \leq k_{\mathrm{hi}}$. For each k the exact natural frequency $\omega_{\mathrm{n},i}$ is identified using:

$$\frac{\partial\,|I\,(n,\,k_i,\,\omega\,)|}{\partial\omega} = 0, \tag{8}$$

where I is defined with Eq. (1) and i is the mode number. The maximum defined with the Eq. (8) is sought using a simple maximum search numerical procedures within a narrow frequency region set around estimated natural frequency, for the n_1 parameter only. The k_i parameter corresponding to a particular mode i is selected by searching for the minimum standard deviation of the damping $\delta_{i,l}(k)$ between selected spatial locations l:

$$k_i = \arg\min_k \left\{ \operatorname*{std}_l \operatorname{dev}\left\{\delta_{i,l}\,(k)\right\}\right\} \tag{9}$$

In step 5, using k_i and $\omega_{\mathrm{n},i}$, the MWDI is continued for the full-field damping identification $\boldsymbol{\delta}_i = \begin{bmatrix}\delta_{i1} & \delta_{i2} & \cdots & \delta_{ij}\end{bmatrix}$ at all measurement locations j (typically, the number of full-field measurement locations is from several hundreds to several thousands).

In step 6, the full-field damping ratios are spatially weighted to obtain the modal damping ratio δ_i. Because the identification near nodal points will be prone to uncertainty due to a low SNR, the weight of these locations has to be reduced. In contrast, damping ratios identified near anti-nodes must have an increased weight. The PSD is a good choice for weighting not only it is easy to obtain, but also because it is related to the square of the identified

deflection shape. The square is selected because the deflection shape is proportional to the mechanical energy (damping energy and noise are expected to be related to a fraction of the mechanical energy) and the square always results in a positive weight. The normalized full-field PSD $\tilde{\mathbf{P}}_i$ for the i-th mode is defined as:

$$\tilde{\mathbf{P}}_i = \begin{bmatrix} \cdots & P_{j-1}(\omega_i) & P_j(\omega_i) & P_{j+1}(\omega_i) & \cdots \end{bmatrix} \Big/ \sum_j P_j(\omega_i) \tag{10}$$

Finally, the spatially weighted modal damping is obtained:

$$\delta_i = \tilde{\mathbf{P}}_i \cdot \boldsymbol{\delta}_i^{\mathrm{T}} \tag{11}$$

4. Experimental research

The spatially weighted MWDI method is here applied to measurements of a freely supported aluminium beam, see Figs. 3 and 4. The beam ($l = 600\,\mathrm{mm}$, $b = 50\,\mathrm{mm}$, $h = 12\,\mathrm{mm}$) was excited with an modal hammer (PCB 086C03) at location $l_{\mathrm{E}} = 400\,\mathrm{mm}$. The response was measured with an accelerometer (DYTRAN 3097A2T) at the location $l_{\mathrm{R}} = 500\,\mathrm{mm}$. Both locations ($l_{\mathrm{E}}$ and l_{R}) are chosen carefully by taking care to avoid nodes for the first five natural frequencies. The full-field displacement response was measured using a high-speed camera (FASTCAM SA-Z type 2100K-M-64GB, 12 bit greyscale sensor).

A data-acquisition (DAQ) card NI-9234 was used to simultaneously acquire (sampling frequency $f_{\mathrm{s}} = 51.2\,\mathrm{kHz}$) signals from the modal hammer, the accelerometer and the voltage trigger. For the voltage trigger, the modal hammer was equipped with an electric wire that, when in contact with the beam, closes the electric circuit and triggers the high-speed camera and the NI-DAQ simultaneously, acting as a software trigger. After the hit, the video is recorded to the high-speed camera's internal memory, signals from modal hammer and accelerometer are recorded on the hard drive including pre-triggered samples. An overview of the measurement chain is shown in Fig. 5. Fig. 6 shows an example of the excitation force and Fig. 7 shows the Frequency Response Function between the response accelerometer and the impact force.

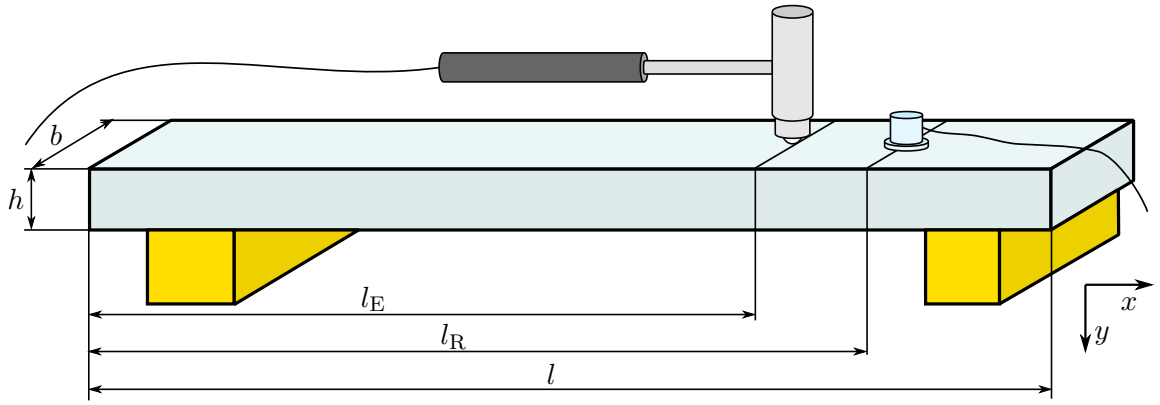

Figure 3: Schematic overview of the beam, not to scale.

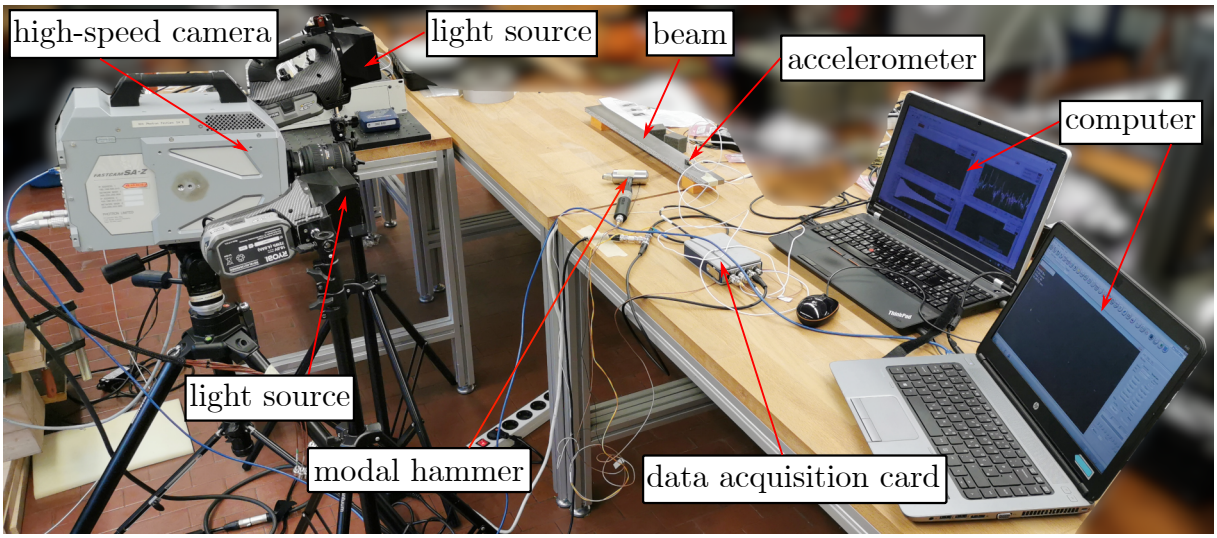

Figure 4: Experimental set-up

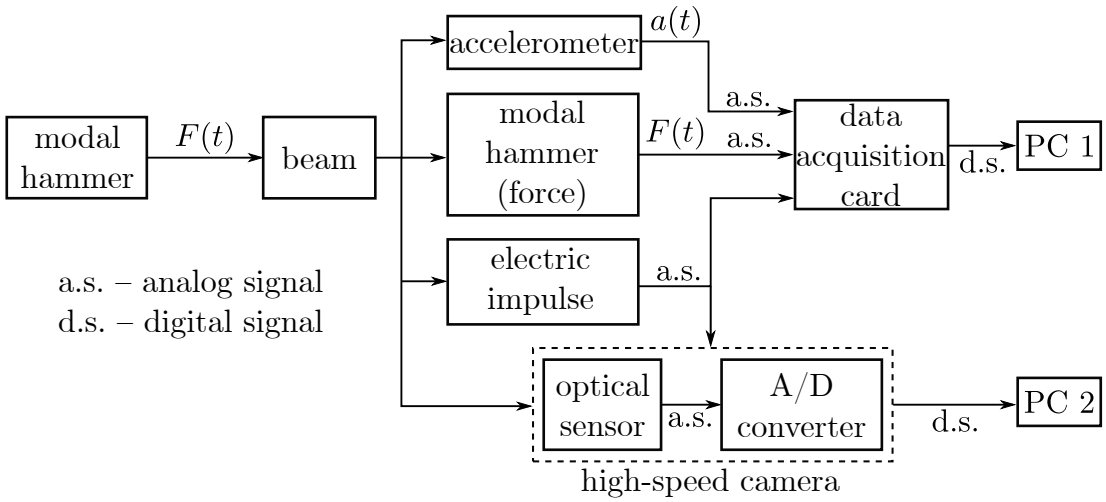

Figure 5: Measurement chain.

4.1. Damping identification from high-speed video data

The displacement from the high-speed video recording (2 s at 50 000 FPS) is detected using the Lucas-Kanade method [35] as implemented in the open-source package pyIDI [36]. The displacement was identified at $194 \times 3 = 582$ locations, based on 12×12 px subsets at a distance of $\Delta x = \Delta y = 5$ px, see Fig. 8. Fig. 9 shows the response displacement (in pixels) identified from the high-speed camera at a single location (top-left point of the beam, see Fig. 8). To clearly show how each mode spreads in the time domain, the continuous wavelet transform is applied to the response using the Gabor wavelet function. The scalogram of the response is shown in Fig. 10. For practical reasons, the CWT is obtained around each mode (±50 Hz) using different wavelet function parameters and the amplitudes around each mode are normalized to 1.

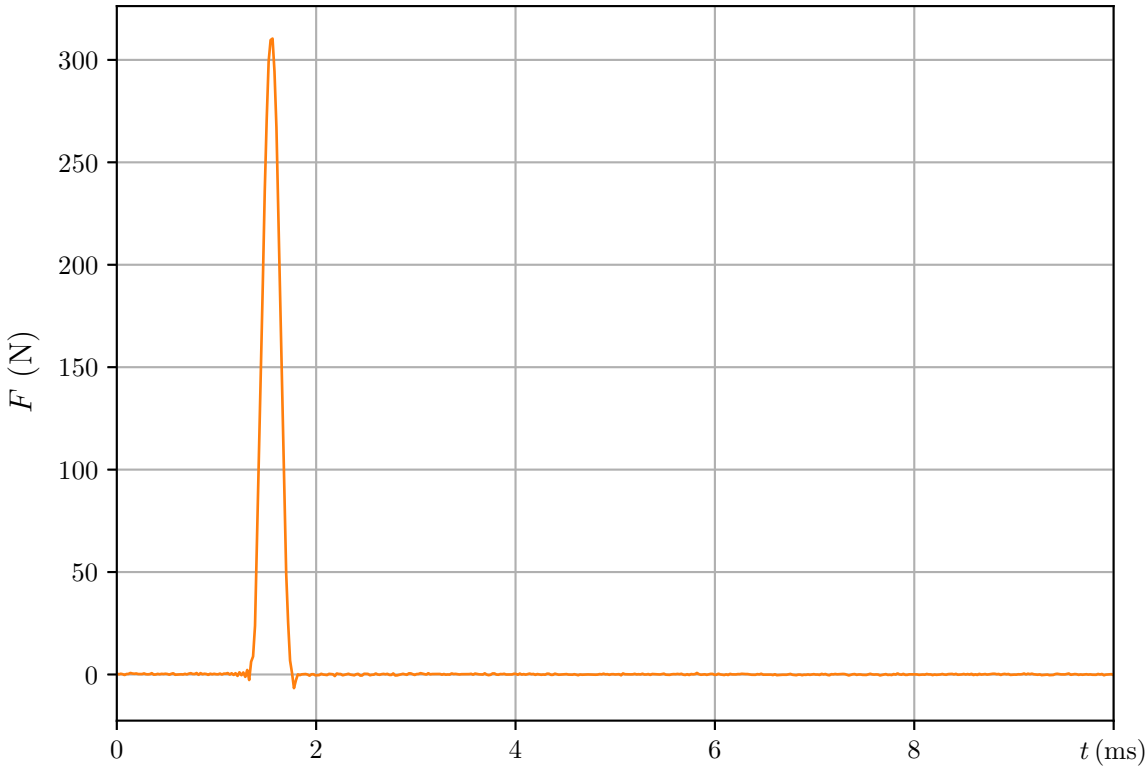

Figure 6: Excitation force.

In Fig. 11 the normalized full-field PSD $\tilde{\mathbf{P}}_i$ (10) is shown for the 1st ($i = 1$) and the 5th ($i = 5$) modes. The spectral separation of PSD is established by using a narrow rectangular window around each natural frequency. From $\tilde{\mathbf{P}}_i$ the locations within the top 1 % values are used for the identification of k_i parameters, as described in step 4, see Sec. 3. In Fig. 10 the dashed line marks the limit between the top 1 % values and the rest. Estimated natural frequencies (Tab. 1) are used as the starting frequencies for the extended MWDI method ($\omega_i = 2\pi\tilde{f}_{\mathrm{n},i}$). Additionally, the parameters $n_1 = 5$ and $n_2 = 10$ are used. The results of the identification in step 4: the k_i parameters and the exactly identified natural frequencies $f_{\mathrm{n},i}$ are shown in Tab. 1.

Table 1: Identification results from the best 1% points using the eMWDI method with parameters $n_1 = 5$, $n_2 = 10$

Natural frequency:	1st	2nd	3rd	4th	5th
estimated: $\tilde{f}_{\mathrm{n}}$ (Hz)	179	482	944	1551	2306
identified: f_{n} (Hz)	179.21	482.22	941.15	1549.1	2304.7
Parameter: k	95	458	570	342	554

Full-field identification using the MWDI method as described in step 5 is based on the parameters identified in step 4: k_i, $f_{\mathrm{n},i}$, n_1, n_2. The results of the full-field damping

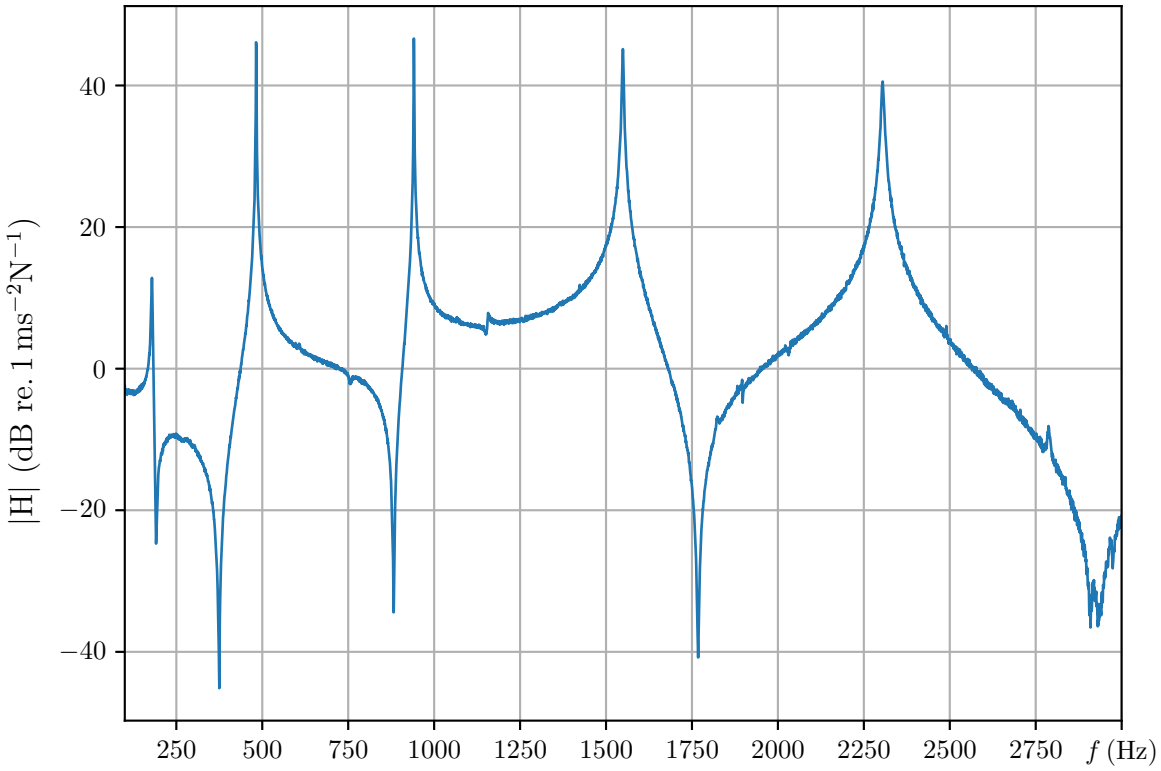

Figure 7: FRF obtained from the response accelerometer and force impulse.

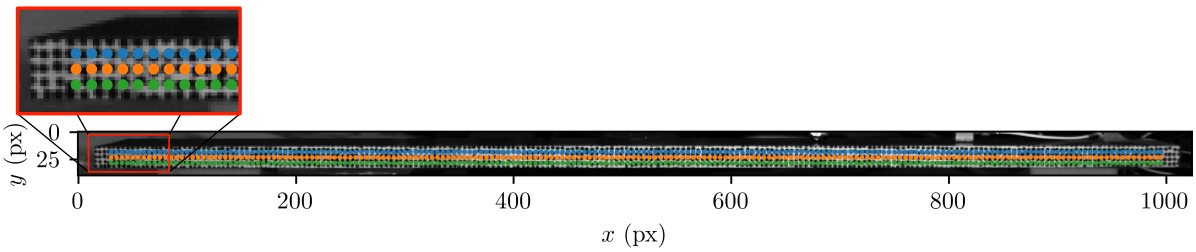

Figure 8: A single frame from the high-speed camera view, showing speckle type and displacement identification points with dots (colours correspond to: blue – top, orange – middle and green – bottom row).

identification $\boldsymbol{\delta}_i$ for all the identified modes are shown in Figs. 12 and 13. Additionally, the normalized full-field PSD $\tilde{\mathbf{P}}_i$ (10) is shown next to the identified damping ratio in Figs. 12 and 13, which confirms that the damping uncertainty is high when the response amplitudes are small and giving arguments for the spatially weighted damping as defined in Eq. (11). The spatially weighted damping ratios are given in Tab. 2.

Table 2: Results of the spatially weighted full-field damping identification.

Natural frequency:	1$^{\text{st}}$	2$^{\text{nd}}$	3$^{\text{rd}}$	4$^{\text{th}}$	5$^{\text{th}}$
δ (%)	0.7508	0.0633	0.0358	0.1041	0.1482

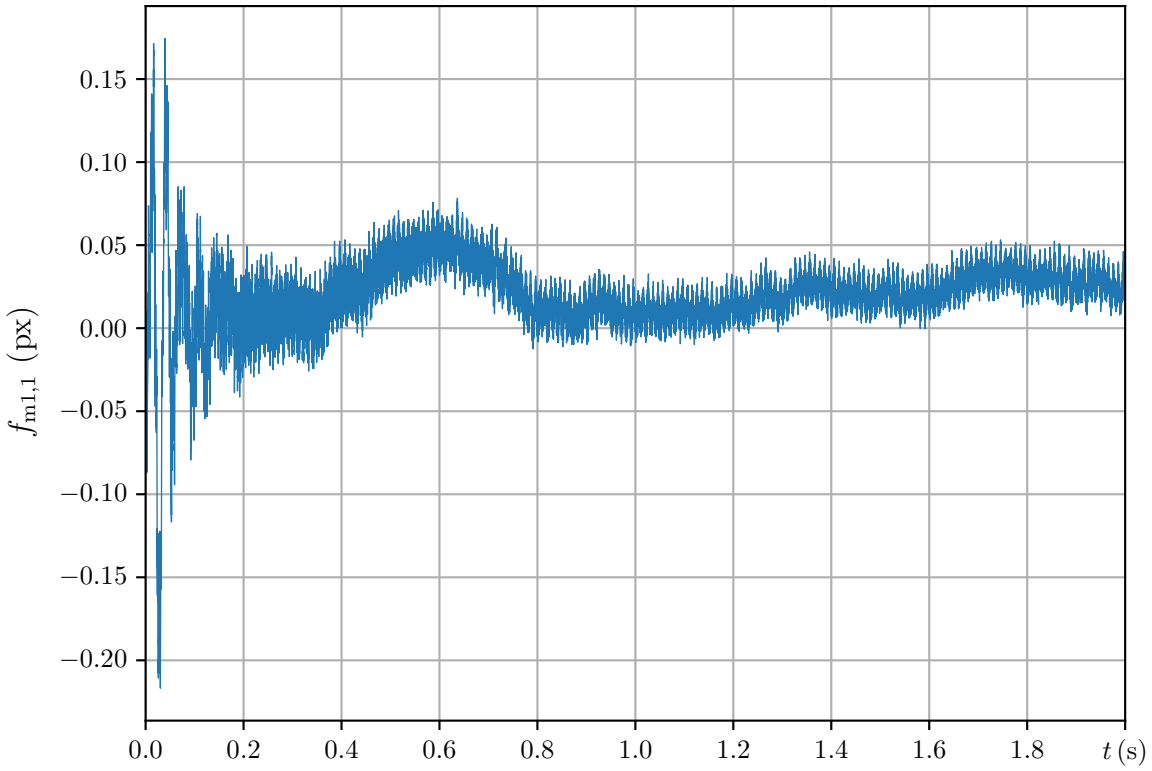

Figure 9: High-speed camera based displacement at a single location.

4.2. Damping identification based on a high dynamic range sensor

In this section the reference damping ratios were obtained from the accelerometer (high-dynamic range), only. In the preliminary research, not reported here, it was found that due to the high-dynamic range of the accelerometer, using more accelerometers and/or different locations, would not have a significant effect on the damping identification. The FRF can be seen in Fig. 7. The identification relies on the MWDI method (step 5) using the same input values as identified in step 4 for the full-field identification of damping (see Tab. 1). The results are shown in Tab. 3. A comparison with the results from Tab. 2, expressed as a relative error calculated with $\text{error}_i = (\delta_i - \delta_{\text{acc},i})/\delta_{\text{acc},i} \cdot 100$ %, is also added to Tab. 3.

Table 3: Identification results based on accelerometer data.

Natural frequency:	1^{st}	2^{nd}	3^{rd}	4^{th}	5^{th}
δ_{acc} (%)	0.7443	0.0633	0.0364	0.1054	0.1567
error (%)	0.87	-0.06	-1.64	-1.21	-5.43

By looking at the error values in Tab. 3 it is clear that the longest error of 5.4 % is as expected at the natural frequency of 2.3 kHz, because the displacement responses of higher modes are typically low and the response from camera is very noisy. This leaves relatively low amount of usefull information to identify damping. The character of the signal can

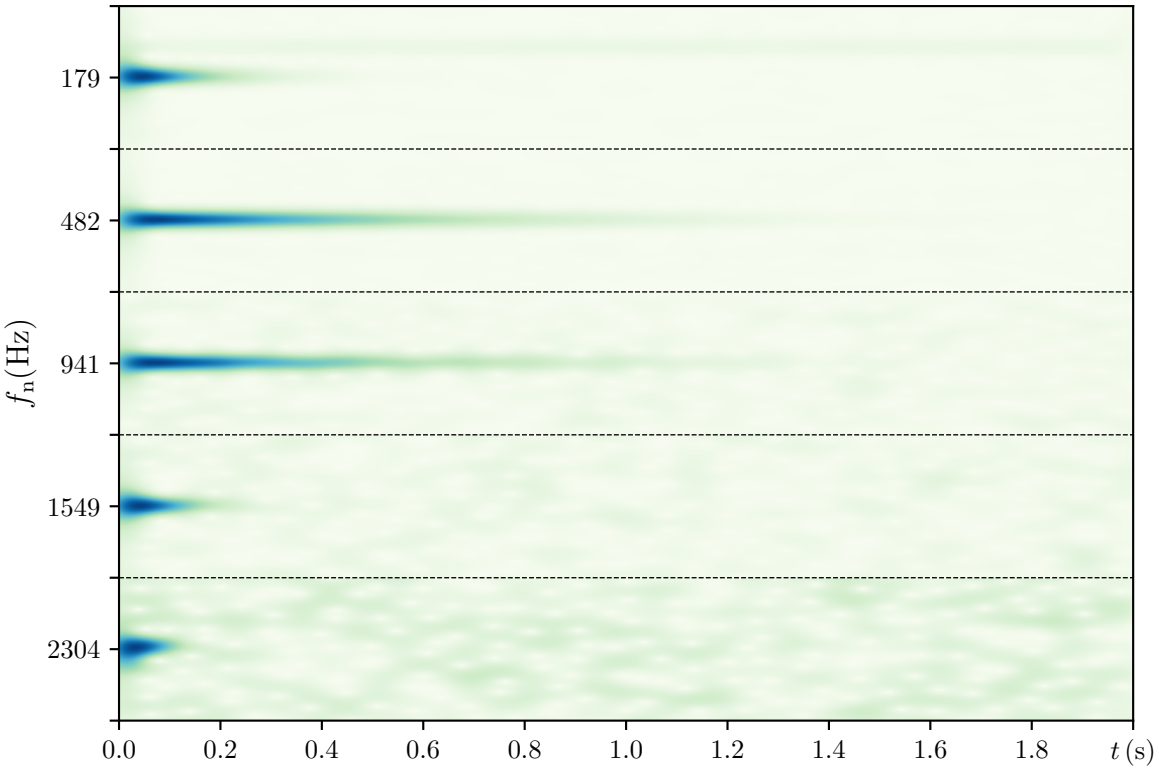

Figure 10: Scalogram of a single location of the high-speed camera based displacement.

be seen in the scalogram in Fig. 10. Therefore, a method that acts like a microscope for signal is required and MWDI is such method. It is important to say that eMWDI method managed to identify adequate k parameter to supply in MWDI method that prefromed well. The errors of the remaining modes are below 2 %. It is clear that the second mode, which was well excited, was accurately identified. The time to perform the identification is mostly determined by step 4, which is the most demanding from the calculation perspective, was $\approx$ 8 min on the processor Intel(R) Core(TM) i3-2350M without executing for loops in parallel. To perform the full-field identification in step 5 on the same CPU required 30 s. The remaining steps executed quickly, in just few seconds.

5. Conclusion

Accurate damping identification is challenging even with high-dynamic-range sensors such as piezoelectric accelerometer. A high-speed camera provides relatively low-dynamic-range measurements, which are also contaminated with measurement noise (typically, 3 out of 8 bits are contaminated with noise). This research focuses on the identification of the damping from measuring camera-based displacements only.

While the camera-based identified displacements are of relatively low quality, the full-field measurement presents an over-determined data set for the spatially invariant damping parameter identification. This research proposed a method for spatially weighted damping

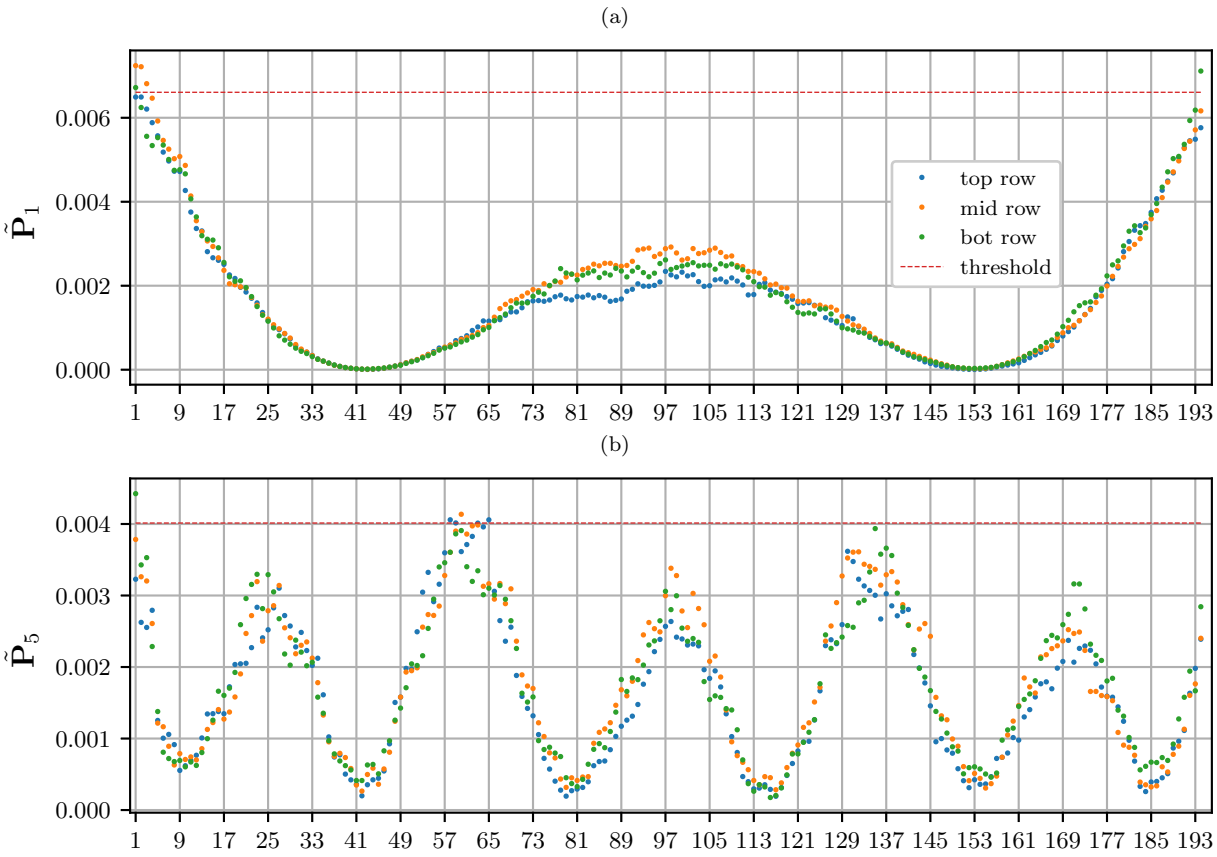

Figure 11: Spatial distribution of the energy spectra for (a) the 1st and (b) the 5th mode.

identification, which takes into account the spatially dependent uncertainty of the damping identification. The method is based on the Morlet Wave Damping Identification (MWDI) method, which has the advantage of being resistant to noise, successful in damping identification at close modes and also numerically fast. The advantages of the MWDI method are especially important for the damping identification and the large number of measurement locations (*i.e.*, in full-field, high-speed-camera-based identification). Tuning the MWDI method's parameters is required, which is established using the extended MDWI method on a fraction of the measurement locations. Finally, to obtain a single damping ratio per each mode, the damping is weight averaged based on the PSD of the full-field response of each mode.

The research involved an aluminium beam that was excited with a single hit from a modal hammer and the response was recorded simultaneously with a high-speed camera and a piezoelectric accelerometer, which was used for a comparison of the identified results. Damping was identified for the natural frequencies up to 2.5 kHz: with the proposed method for the high-speed-camera measurements and with the MWDI method for the piezoelectric accelerometer measurement. A comparison of the results with the accelerometer confirmed similar results: four damping ratios were identified within approximately 1 % when compared to the accelerometer results; the damping ratio at 2304.7 Hz was identified within

approximately 5 % when compared to the accelerometer result.

This research confirmed that the full-field high-speed-camera-based damping identification approach can result in a similar accuracy of damping identification to an identification

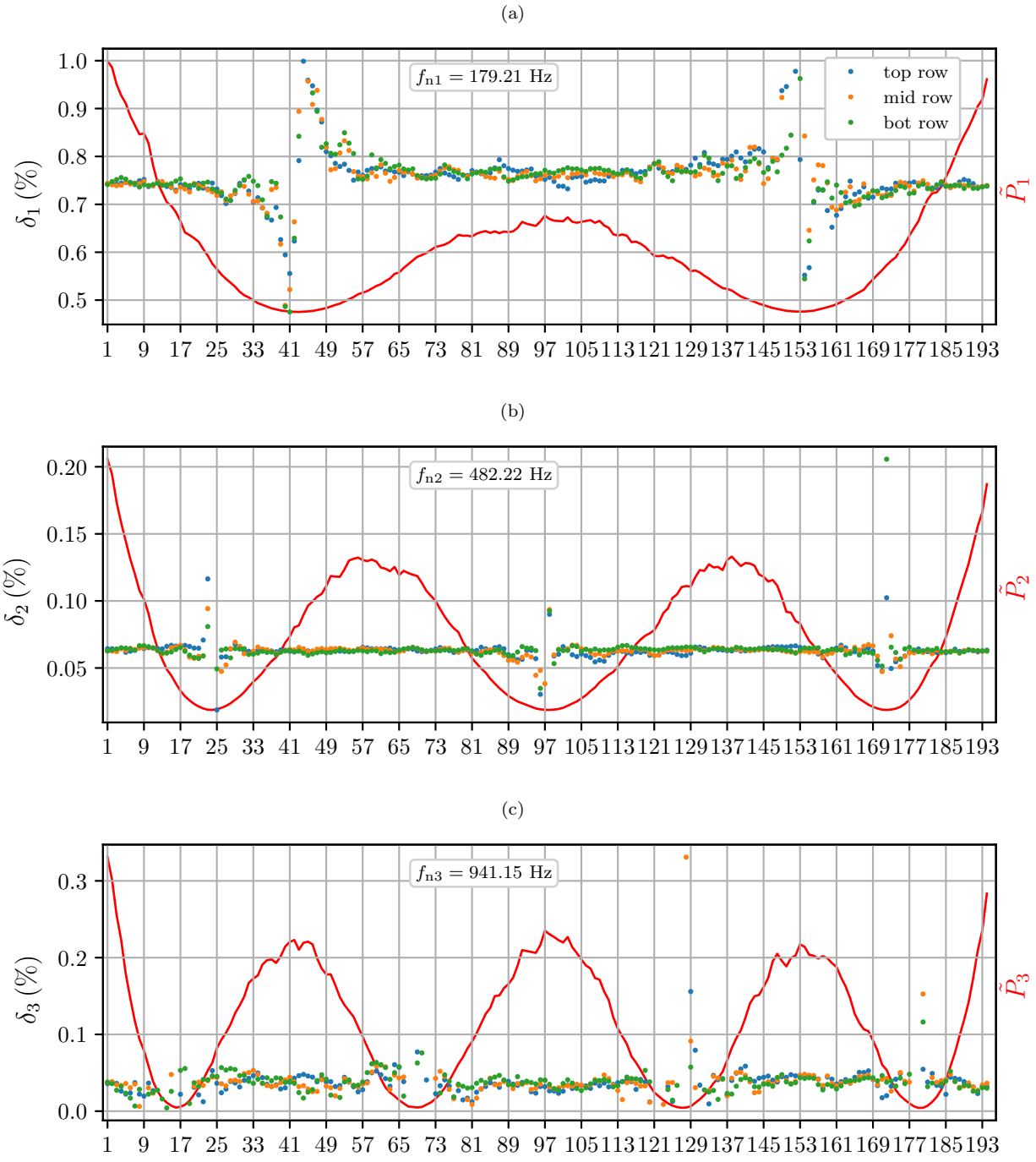

Figure 12: Damping identified at all spatial points using MW method: a) Mode 1, b) Mode 2, c) Mode 3.

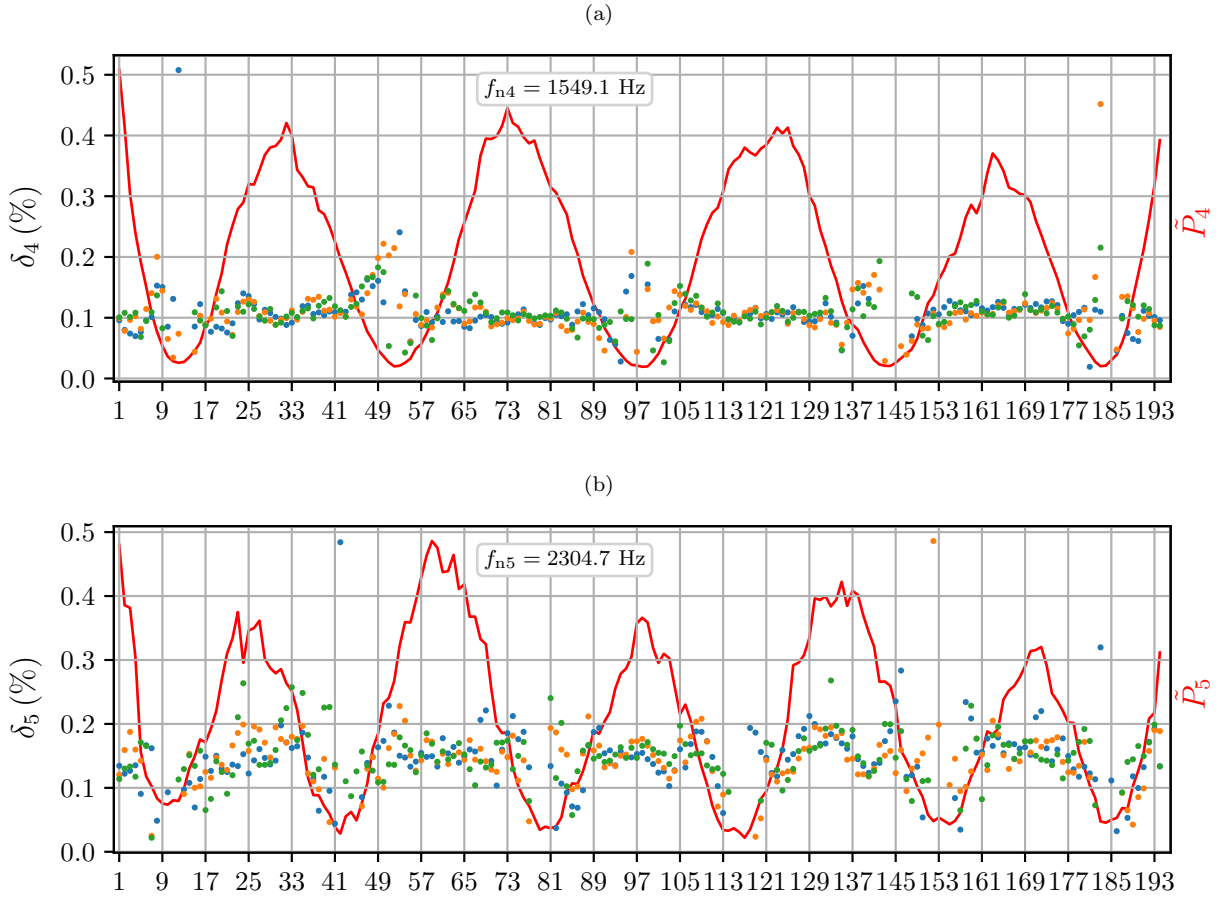

Figure 13: Damping identified at all spatial points using MW method: a) Mode 4, b) Mode 5.

based on high-dynamic-range sensors. With this, the highly accurate, non-contact identification of damping based on camera measurements is confirmed, opening up new possibilities in structural health monitoring and failure analysis.

Acknowledgement

The authors acknowledge partial financial support from the European Union's Horizon 2020 research and innovation programme under the Marie Skłodowska-Curie grant agreement No 101027829, the Slovenian Research Agency (J2-1730) and the Croatian Science Foundation (HRZZ-IP-2018-01-6774). The authors would also like to acknowledge the experimental help of Klemen Zaletelj and Domen Gorjup.

Appendix A. Definition of a SDOF example

Parameters that describe a SDOF system used as the example in the text are:

- system: $m = 1$ kg, $k = 320$ kN m^{-1}, $c = 11.31$ N s m^{-1}

- initial condition: $v_0 = 1\ \mathrm{m\,s^{-1}}$
- modal parameters: $f_\mathrm{n} = 90$ Hz, $\delta = 1\ \%$
- signal: $f_\mathrm{s} = 8000\ \mathrm{S\,s^{-1}}$, $T = 0.5$ s

References

[1] M. N. Helfrick, C. Niezrecki, P. Avitabile, T. Schmidt, 3d digital image correlation methods for full-field vibration measurement, Mechanical Systems and Signal Processing 25 (2011) 917–927. doi:10.1016/j.ymssp.2010.08.013.

[2] T. Siebert, R. Wood, K. Splitthof, High speed image correlation for vibration analysis, Journal of Physics: Conference Series 181 (2009) 012064. doi:10.1088/1742-6596/181/1/012064.

[3] T. Durand-Texte, M. Melon, E. Simonetto, S. Durand, M.-H. Moulet, Single-camera single-axis vision method applied to measure vibrations, Journal of Sound and Vibration 465 (2020) 115012. doi:10.1016/j.jsv.2019.115012.

[4] T. J. Beberniss, D. A. Ehrhardt, High-speed 3d digital image correlation vibration measurement: Recent advancements and noted limitations, Mechanical Systems and Signal Processing 86 (2017) 35–48. doi:10.1016/j.ymssp.2016.04.014.

[5] J. Baqersad, P. Poozesh, C. Niezrecki, P. Avitabile, Photogrammetry and optical methods in structural dynamics – a review, Mechanical Systems and Signal Processing 86 (2017) 17–34. doi:10.1016/j.ymssp.2016.02.011.

[6] P. J. Sousa, F. Barros, P. J. Tavares, P. M. Moreira, Digital image correlation displacement measurement of a rotating rc helicopter blade, Engineering Failure Analysis 90 (2018) 371–379. doi:10.1016/j.engfailanal.2018.04.005.

[7] P. Maljaars, L. Bronswijk, J. Windt, N. Grasso, M. Kaminski, Experimental validation of fluid–structure interaction computations of flexible composite propellers in open water conditions using bem-fem and rans-fem methods, Journal of Marine Science and Engineering 6 (2018). doi:10.3390/jmse6020051.

[8] Z. Su, J. Pan, S. Zhang, S. Wu, Q. Yu, D. Zhang, Characterizing dynamic deformation of marine propeller blades with stroboscopic stereo digital image correlation, Mechanical Systems and Signal Processing 162 (2022) 108072. doi:10.1016/j.ymssp.2021.108072.

[9] J. Baqersad, C. Niezrecki, P. Avitabile, Full-field dynamic strain prediction on a wind turbine using displacements of optical targets measured by stereophotogrammetry, Mechanical Systems and Signal Processing 62-63 (2015) 284–295. doi:10.1016/j.ymssp.2015.03.021.

[10] P. Poozesh, A. Sabato, A. Sarrafi, C. Niezrecki, P. Avitabile, R. Yarala, Multicamera measurement system to evaluate the dynamic response of utility-scale wind turbine blades, Wind Energy 23 (2020) 1619–1639. doi:10.1002/we.2505.

[11] C.-Y. Chang, C.-W. Huang, Non-contact measurement of inter-story drift in three-layer rc structure under seismic vibration using digital image correlation, Mechanical Systems and Signal Processing 136 (2020) 106500. doi:10.1016/j.ymssp.2019.106500.

[12] L. Ngeljaratan, M. A. Moustafa, Structural health monitoring and seismic response assessment of bridge structures using target-tracking digital image correlation, Engineering Structures 213 (2020) 110551. doi:10.1016/j.engstruct.2020.110551.

[13] R. Wu, D. Zhang, Q. Yu, Y. Jiang, D. Arola, Health monitoring of wind turbine blades in operation using three-dimensional digital image correlation, Mechanical Systems and Signal Processing 130 (2019) 470–483. doi:10.1016/j.ymssp.2019.05.031.

[14] D. A. Ehrhardt, M. S. Allen, S. Yang, T. J. Beberniss, Full-field linear and nonlinear measurements using continuous-scan laser doppler vibrometry and high speed three-dimensional digital image correlation, Mechanical Systems and Signal Processing 86 (2017) 82–97. doi:10.1016/j.ymssp.2015.12.003, full-field, non-contact vibration measurement methods: comparisons and applications.

[15] J. Javh, J. Slavič, M. Boltežar, High frequency modal identification on noisy high-speed camera data, Mechanical Systems and Signal Processing 98 (2018) 344–351. doi:10.1016/j.ymssp.2017.05.008.

[16] T. Schmidt, J. Tyson, K. Galanulis, Full-field dynamic displacement and strain measurement using advanced 3d image correlation photogrammetry: Part 1, Experimental Techniques 27 (2003) 47–50. doi:10.1111/j.1747-1567.2003.tb00115.x.

[17] Y. Yang, C. Dorn, T. Mancini, Z. Talken, G. Kenyon, C. Farrar, D. Mascareñas, Blind identification

of full-field vibration modes from video measurements with phase-based video motion magnification, Mechanical Systems and Signal Processing 85 (2017) 567–590. doi:10.1016/j.ymssp.2016.08.041.

[18] L. Yu, B. Pan, Single-camera high-speed stereo-digital image correlation for full-field vibration measurement, Mechanical Systems and Signal Processing 94 (2017) 374–383. doi:10.1016/j.ymssp.2017.03.008.

[19] R. Huňady, M. Hagara, A new procedure of modal parameter estimation for high-speed digital image correlation, Mechanical Systems and Signal Processing 93 (2017) 66–79. doi:10.1016/j.ymssp.2017.02.010.

[20] K. Ege, N. Roozen, Q. Leclère, R. G. Rinaldi, Assessment of the apparent bending stiffness and damping of multilayer plates; modelling and experiment, Journal of Sound and Vibration 426 (2018) 129–149. doi:10.1016/j.jsv.2018.04.013.

[21] L. Felipe-Sesé, Ángel J. Molina-Viedma, E. López-Alba, F. A. Díaz, Fp+dic for low-cost 3d full-field experimental modal analysis in industrial components, Mechanical Systems and Signal Processing 128 (2019) 329–339. doi:10.1016/j.ymssp.2019.04.004.

[22] Y. Yang, C. Dorn, Affinity propagation clustering of full-field, high-spatial-dimensional measurements for robust output-only modal identification: A proof-of-concept study, Journal of Sound and Vibration 483 (2020) 115473. doi:10.1016/j.jsv.2020.115473.

[23] M. Silva, B. Martinez, E. Figueiredo, J. C. Costa, Y. Yang, D. Mascareñas, Nonnegative matrix factorization-based blind source separation for full-field and high-resolution modal identification from video, Journal of Sound and Vibration 487 (2020) 115586. doi:10.1016/j.jsv.2020.115586.

[24] F. Marchetti, K. Ege, Q. Leclère, N. Roozen, On the structural dynamics of laminated composite plates and sandwich structures; a new perspective on damping identification, Journal of Sound and Vibration 474 (2020) 115256. doi:10.1016/j.jsv.2020.115256.

[25] J. Slavič, M. Boltežar, Damping identification with the morlet-wave, Mechanical Systems and Signal Processing 25 (2011) 1632–1645. doi:10.1016/j.ymssp.2011.01.008.

[26] W. J. Staszewski, Identification of damping in mdof systems using time-scale decomposition, Journal of sound and vibration 203 (1997) 283–305. doi:10.1006/jsvi.1996.0864.

[27] J. Slavič, I. Simonovski, M. Boltežar, Damping identification using a continuous wavelet transform, application to real data, Journal of Sound and Vibration 262 (2003) 291–307. doi:10.1016/S0022-460X(02)01032-5.

[28] I. Tomac, Ž. Lozina, D. Sedlar, Extended morlet-wave damping identification method, International Journal of Mechanical Sciences 127 (2017) 31 – 40. doi:10.1016/j.ijmecsci.2017.01.013.

[29] M. Ruzzene, A. Fasana, L. Garibaldi, B. Piombo, Natural frequencies and dampings identification using wavelet transform: application to real data, Mechanical systems and signal processing 11 (1997) 207–218. doi:10.1006/mssp.1996.0078.

[30] P. Goupillaud, A. Grossmann, J. Morlet, Cycle-octave and related transforms in seismic signal analysis, Geoexploration 23 (1984) 85 – 102. doi:10.1016/0016-7142(84)90025-5.

[31] S. Mallat, A Wavelet Tour Of Signal Processing, 2nd ed., Academic Press, San Diego, 1999.

[32] D. Gorjup, J. Slavič, A. Babnik, M. Boltežar, Still-camera multiview spectral optical flow imaging for 3d operating-deflection-shape identification, Mechanical Systems and Signal Processing 152 (2021) 107456. doi:10.1016/j.ymssp.2020.107456.

[33] R. Del Sal, L. Dal Bo, E. Turco, A. Fusiello, A. Zanarini, R. Rinaldo, P. Gardonio, Structural vibration measurement with multiple synchronous cameras, Mechanical Systems and Signal Processing 157 (2021) 107742. doi:10.1016/j.ymssp.2021.107742.

[34] J. S. Bendat, A. G. Piersol, Random data: analysis and measurement procedures, volume 729, John Wiley & Sons, 2011.

[35] B. D. Lucas, T. Kanade, Iterative image registration technique with an application to stereo vision, in: Proceedings of the 7th International Joint Conference on Artificial Intelligence, volume 2, 1981, pp. 674–679.

[36] K. Zaletelj, D. Gorjup, J. Slavič, ladisk/pyidi: Release of the version v0.23, 2020. URL: https://doi.org/10.5281/zenodo.4017153. doi:10.5281/zenodo.4017153.